Journal of Communications Technology and Electronics, Vol. 49, No. 9, 2004, pp. 1051–1059. Translated from Radiotekhnika i Elektronika, Vol. 49, No. 9, 2004, pp. 1118–1127.

MICROWAVE ELECTRONICS

Joint Oscillations, Including Synchronization Processes, in Backward-Wave Gyrooscillators with Coupled Electrodynamic Systems

A. A. Koronovskii, D. I. Trubetskov, and A. E. Hramov

Received November 1, 2002

Abstract—Oscillation synchronization in backward-wave gyrotubes with coupled waveguiding systems (CWGS gyro-BWTs) is investigated for the first time. It is shown that two bistability states occur in a CWGS BWT, depending on the character of oscillations excited in the system. The characteristics of joint spatial–temporal oscillations in a coupled system are studied. Physical processes observed during self-oscillatory system locking are considered.

Recently, much attention has been given to generation and amplification of high-frequency electromagnetic oscillations provided by interaction between spiral electron beams and waveguide traveling waves (cyclotron-resonance masers) [1–10]. Based on the interaction of the beam and a direct wave (traveling-wave gyrotubes, or gyro-TWTs) or backward (counter-propagating) wave (backward-wave gyrotubes, or gyro-BWTs), these systems are regarded as the most promising millimeter-wave amplifiers and oscillators. In this work, we consider a model based on the interaction of a backward wave and spiral beam electron oscillators. When the electron and counter-propagating electromagnetic waves in a regular waveguide are synchronized, i.e., when

$$\omega \approx \hat{\omega}, \quad \hat{\omega} - \beta_0(\hat{\omega}) v_{\parallel} - \omega_c = 0 \qquad (1)$$

this gyro-BWT system produces RF oscillations [11–16]. Here, $\hat{\omega}$ is the synchronization frequency, ω_c is the cyclotron frequency, $v_{\parallel}$ is the electron longitudinal velocity, i.e., the velocity aligned with the applied magnetic field, $\beta_0(\hat{\omega}) = \pm \frac{\omega_{cr}}{c}\sqrt{(\omega/\omega_{cr})^2 - 1}$ is the propagation constant for a waveguide with no electron flow, and ω_{cr} is the cutoff frequency of the mode under consideration (see the dispersion diagram in Fig. 1).

A gyro-BWT is capable of generating power as high as several tens of megawatts at millimeter- and submillimeter-wavelengths, and its frequency can be easily adjusted by varying the longitudinal electron velocity or magnetostatic field [1, 17]. One disadvantage of a gyro-BWT is its low efficiency, which does not exceed 20% [18]. Such a low efficiency is due to the special features of interaction between the beam electron oscillators and the RF field developing along the interaction space: an RF wave travels counter to the beam, and electron oscillators are bunched in a strong output field. The beam debunches as rapidly as it bunches, and the debunching time is not sufficient for energy transfer to the field. Next, a secondary phase bunching occurs over the system's length. This repeated bunching causes multihumped current and field distributions, which are typical of gyro-BWTs [8, 19]. As a result, with an increase in the system's length or in beam current, output signal automodulation is rapidly initiated in a gyro-BWT and the oscillation spectrum becomes multifrequency [18, 19]. By applying gyro-BWTs that interact through coupled waveguiding systems (CWGSs), one can increase the output power, single-frequency oscillation being maintained. In coupled electrodynamic systems, distributed coupling takes place, because the

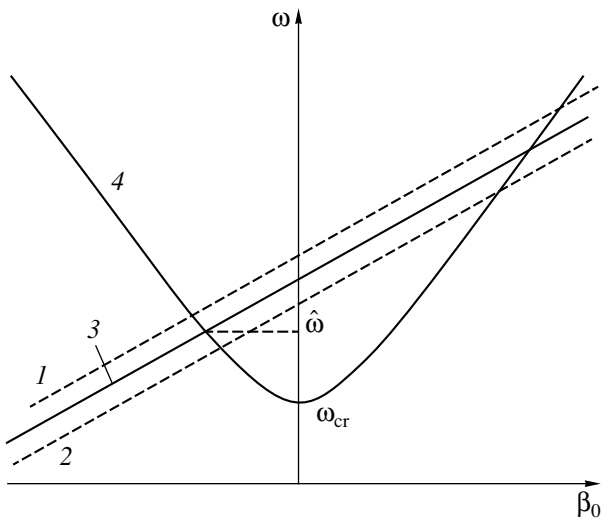

Fig. 1. Beam and waveguide mode dispersion curves for oscillations realized in a backward-wave CRM: curves corresponding to the (*1*) slow I_s and (*2*) fast I_f electron waves, (*3*) spiral beam, and (*4*) waveguide mode dispersion curve determined by the formula $\omega = \sqrt{\omega_{cr}^2 + \beta_0^2 c^2}$.

beam in one of the gyro-BWTs is affected by the electromagnetic wave in the other gyrotube along the entire interaction space. Coupled waveguide systems may be implemented as, e.g., two circular waveguides coupled through slots oriented along the direction of the wave propagation in each of the electrodynamic systems. Increasing the separation between the structures or the width of the coupling slot can vary the coupling parameters.

The use of CWGSs in long-term interaction devices has been considered as applied to *O*-type amplifiers and oscillators (TWTs and BWTs) [20–22]. It should be noted that amplifiers and oscillators with long-term interaction CWGSs may generate a complex stochastic signal, which allows us to consider a system of coupled gyro-BWTs as a possible source of a narrowband millimeter-wave chaotic signal.

In this paper, using numerical simulation, we investigate self-oscillations in coupled gyro-BWTs within the framework of the proposed mathematical model. In particular, we analyze self-oscillation synchronization and complex joint oscillations in a coupled system.

1. MATHEMATICAL MODEL

Let us derive equations describing signal amplification and generation in CWGS gyro-BWTs. We assume that the electromagnetic field is uniform over the electron beam cross section. We ignore the interaction between spiral beam electron oscillators and the RF components of the magnetic field, which implies a constant longitudinal electron flow velocity, $v_\parallel \approx \text{const}$. We also assume that, over the operating frequency band, only the interaction of a spiral beam with the counter-propagating wave can be taken into account. Let a spiral electron beam pass through each of two weakly coupled waveguiding systems. Then, in the stationary case, field amplitudes E_1 and E_2 in these systems satisfy the equations [23, 24]

$$\frac{dE_1}{dx} + j\beta_0 E_1 + \alpha_1 E_2 = i_1, \tag{2}$$

$$\frac{dE_2}{dx} + j\beta_0 E_2 + \alpha_2 E_1 = i_2. \tag{3}$$

Here, quantities $i_{1,2}$ are proportional to the amplitudes of the RF currents of the spiral electron beams and $\alpha_{1,2}$ are the coupling parameters.

Since the systems are identical, $|\alpha_1| = |\alpha_2| = \hat{\alpha}$, and it follows from the law of power flux conservation at $i_1 = i_2 = 0$ that $\alpha_1 = -\alpha_2^* = j\hat{\alpha}$.

Let us represent Eqs. (2) and (3) in the form of normal waves:

$$\frac{dE_s}{dx} + j(\beta_0 + \hat{\alpha})E_s = i_1 + i_2, \tag{4}$$

$$\frac{dE_f}{dx} + j(\beta_0 - \hat{\alpha})E_f = i_1 - i_2. \tag{5}$$

Here, $E_s = E_1 + E_2$ is the amplitude of a slow normal wave (its propagation constant is $\beta_s = \beta_0 + \hat{\alpha}$, and β_0 is the propagation constant of a counter-propagating wave at the frequency of cold synchronism) and $E_f = E_2 - E_1$ is the amplitude of a fast ($\beta_f = \beta_0 - \hat{\alpha}$) normal wave supported by the coupled system.

Let us change to new variables, $\hat{E}_f = E_f \exp[-j\beta_f x]$ and $\hat{E}_s = E_s \exp[-j\beta_s x]$, in system of equations (4), (5) and employ the following normalization of the variables. Let $\xi = \beta_0(\hat{\omega})\varepsilon x$ be a dimensionless coordinate and $\tau = \hat{\omega}\varepsilon(t - x/v_\parallel)(1 + v_\parallel/|v_g|)^{-1}$ be dimensionless time; $F_{f,s} = \hat{E}_{f,s}/2\varepsilon^2 V_0 \beta_0$; $I_{1,2} = (2i_{1,2}/\beta_0^2 KI_0)\exp[-j\beta_0 x]$; and $\alpha = \hat{\alpha}/\beta_0\varepsilon$, where $\varepsilon = \sqrt{I_0 K/4V_0(1 + v_{\perp 0}^2/v_\parallel^2)}$ is the interaction parameter, K is the coupling impedance, and $v_{\perp 0}$ is the initial transverse electron velocity.

In this case, passing from stationary to nonstationary equations [25], we obtain the following system of equations for slowly varying complex amplitudes of the fast and slow waves in the dimensionless variables:

$$\frac{\partial F_s}{\partial \tau} - \frac{\partial F_s}{\partial \xi} = -I_s, \tag{6}$$

$$\frac{\partial F_f}{\partial \tau} - \frac{\partial F_f}{\partial \xi} = -I_f, \tag{7}$$

which determines field functions in the problem of signal amplification and generation by CWGS gyro-BWTs (the field part of the problem). Normal waves $F_{f,s}$ of the system are related to fields $F_{1,2}$ of each of the waveguiding systems by the relationships

$$\begin{aligned} F_s &= (F_1 + F_2)\exp(j\alpha\xi), \\ F_f &= (F_2 - F_1)\exp(-j\alpha\xi). \end{aligned} \tag{8}$$

Slow and fast current waves $I_{f,s}$ are introduced by analogy with expressions (8) and defined as

$$\begin{aligned} I_s &= (I_1 + I_2)\exp(j\alpha\xi), \\ I_f &= (I_2 - I_1)\exp(-j\alpha\xi). \end{aligned} \tag{9}$$

System of equations (6), (7) is solved under the fol-

lowing initial and boundary conditions:

$$F_{1,2}(\xi, \tau = 0) = f^0_{1,2}(\xi), \quad F_{1,2}(\xi = A, \tau) = 0, \quad (10)$$

where A is the dimensionless length of the system and function $f^0_{1,2}$ specifies the initial field distribution along the length of either tube.

Now, let us consider the electron part of the problem. Yulpatov [14, 15] was the first to obtain the equations of motion of electrons in weakly relativistic spiral beams in the presence of an electromagnetic field. For the beams passed through either electrodynamic system, these equations can be represented in terms of the variables introduced above as

$$\frac{d\beta_1}{d\xi} - j\mu_1(1 - |\beta_1|^2)\beta_1 = \frac{1}{2}(F_s\exp[-j\alpha\xi] - F_f\exp[j\alpha\xi]), \quad (11)$$

$$\frac{d\beta_2}{d\xi} - j\mu_2(1 - |\beta_2|^2)\beta_2 = \frac{1}{2}(F_s\exp[-j\alpha\xi] + F_f\exp[j\alpha\xi]), \quad (12)$$

where $\beta_{1,2} = r_{1,2}\exp[j\theta_{1,2}]$ is the complex radius of the electron trajectories for either electron beam and $\mu_{1,2}$ are the anisochronism parameters of the electron oscillator of the first and second flows, respectively. Initially, the electron trajectories are uniformly phase-distributed relative to the RF field, $\beta_{1,2}(\xi = 0) = \exp[j\theta_0]$ ($\theta_0 \in [0, 2\pi]$). The anisochronism parameter is related to the relativistic energy dependence of the mass of electrons and determines the inertia of the system. Amplitudes of the beam RF currents $I_{1,2}$ flowing through each of the waveguiding structures are determined by the relationships

$$I_{1,2} = \frac{1}{2\pi}\int_0^{2\pi}\beta_{1,2}d\theta_0. \quad (13)$$

Thus, the control parameters of the proposed model are system length A, anisochronism parameters $\mu_{1,2}$, and coefficient of coupling between the waveguiding structures α. In the case of a system with a constant beam current of I_0, a variation in A at constant $\mu_{1,2}$ corresponds to a variation in system length l. When l is constant and A is varied by means of varying current I_0, the parameters ($\mu_{1,2}A$) remain constant.

2. MULTISTABILITY AND TRANSIENT PROCESSES IN A SYSTEM OF COUPLED GYRO-BWTS

Let us analyze the dynamics of a CWGS gyro-BWT simulated using nonlinear nonstationary equations (6)–(12). The equations were solved numerically. To this end, we applied the large particle method, a two-step predictor–corrector scheme to integrate the equations of motion, and the Lax–Wendroff integration approach to integrate the equations of normal wave excitation (partial differential equations), which are of the second order of accuracy [26, 27].

The analysis has shown that a gyro-BWTs coupled via waveguiding systems exhibits multistability (or, more precisely, bistability). This effect is observed when, depending on initial conditions, the coupled system goes to one of two stable states that are characterized by different distributions of the RF field and current over the interaction space and, accordingly, by different output powers and generation efficiencies.

Each of the states corresponds to the prevailing either fast or slow normal wave excited in the coupled system at the initial moment. The easiest method of describing this situation involves initial conditions specified as

$$F_s(\tau = 0, \xi) = \delta^0\cos(\pi(A - \xi)/2), \quad F_f(\tau = 0, \xi) = 0 \quad (14)$$

or

$$F_s(\tau = 0, \xi) = 0, \quad F_f(\tau = 0, \xi) = \delta^0\cos(\pi(A - \xi)/2), \quad (15)$$

where δ^0 is the amplitude of an initial perturbation.

The state that is realized in the system when the initial distribution is specified in form (14) (i.e., when excitation of the slow normal wave prevails) is referred to as a slow state. The state that is realized when the distribution is specified in form (15) is referred to as a fast state.

To illustrate multistability in the CWGS gyro-BWTs, the distributions of the RF current and field in one of the coupled gyro-BWTs are shown in Fig. 2. The curves correspond to the same control parameters and different initial conditions specified by expressions (14) and (15), respectively. From the presented plots of F_1 and I_1, it follows that fundamentally different oscillation modes are realized at the same control parameters. These modes are characterized by topologically different current and field distributions depending on which of the normal waves (slow or fast one) prevails at the initial moment $\tau = 0$.

Under different multistable conditions, joint RF oscillations are excited in the coupled system at different frequencies. Figure 3 shows the oscillation frequency (solid line) versus the coupling coefficient between the wave-guiding structures α for the fast and slow states of the coupled system at the same control parameters of the gyro-BWTs ($\mu_1 = \mu_2 = 2.0$). It can be

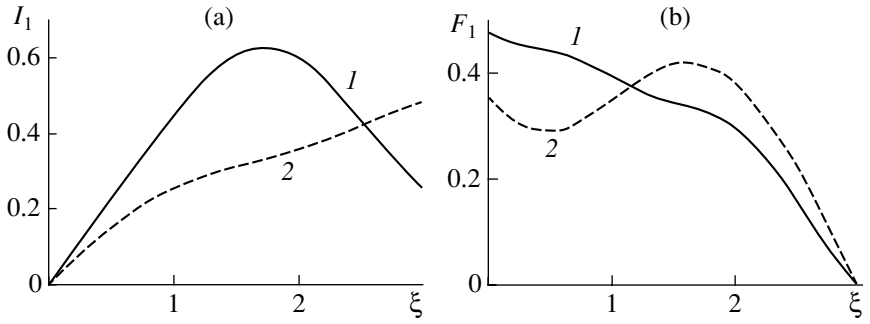

Fig. 2. Stationary distributions of RF current I_1 and field F_1 at $A = 3.0$, $\mu_1 = 2.0$, $\mu_2 = 3.0$, and $\alpha = 0.8$ obtained under initial conditions (a) (14) and (b) (15); (*1*) fast state and (*2*) slow state. The initial perturbation amplitude is $\delta^0 = 0.01$.

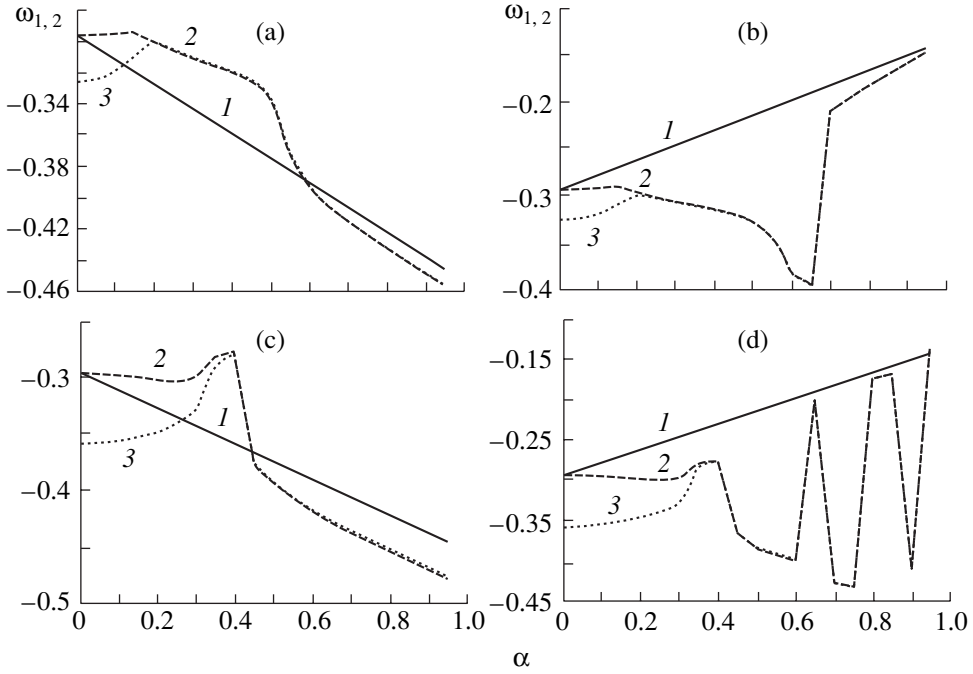

Fig. 3. Frequency generated by each of the CWGS gyro-BWTs vs. the coupling coefficient determined at the system lengths $A =$ (a, b) 3.0 and (c, d) 4.0 for the (a, c) fast and slow (b, d) states of the system: (*1*) $\mu_1 = \mu_2 = 2.0$, (*2*) $\mu_1 = 2.0$, and (*3*) $\mu_2 = 3.0$.

seen that, as the coupling intensifies, the oscillation frequency decreases in the fast state, whereas it increases in the slow state. Such a behavior of the oscillation frequency is related to the shape of the waveguide dispersion curve. The presence of coupling between the waveguiding structures changes the propagation velocity of the normal waves supported by the system. The dispersion curve for slow wave I_s, which is sustained by the electron beam, passes above the dispersion curve for the beam $\omega - \beta_0 v_\parallel - \omega_c = 0$ (see Fig. 1, curve *1*); therefore, the synchronism frequency for the electromagnetic and slow normal waves is higher than for the electromagnetic and electron waves in the absence of coupling. A reverse situation occurs when excitation of fast normal wave I_f prevails. In this case, the dispersion curve is located below the dispersion curve for the beam (see Fig. 1, curve *2*) and the oscillation frequency is lower than in the uncoupled system.

It should be noted that the discovered multistability (bistability) in a system of two coupled gyro-BWTs is similar to the process of competition between oscillations observed when the realized oscillation mode is determined by the initial conditions, which is a well-known effect in the theory of oscillation and waves [28]. The multistability phenomenon has been described in detail both for elementary dynamic systems (mappings) [29, 30] and for distributed self-oscillatory systems, including nonlinear optical devices and microwave electronic systems (free electron lasers, gyrotrons with a nonfixed field structure, etc.) [31–33].

Specification of the initial conditions in the form of Eqs. (14) or (15) does not allow us to determine which

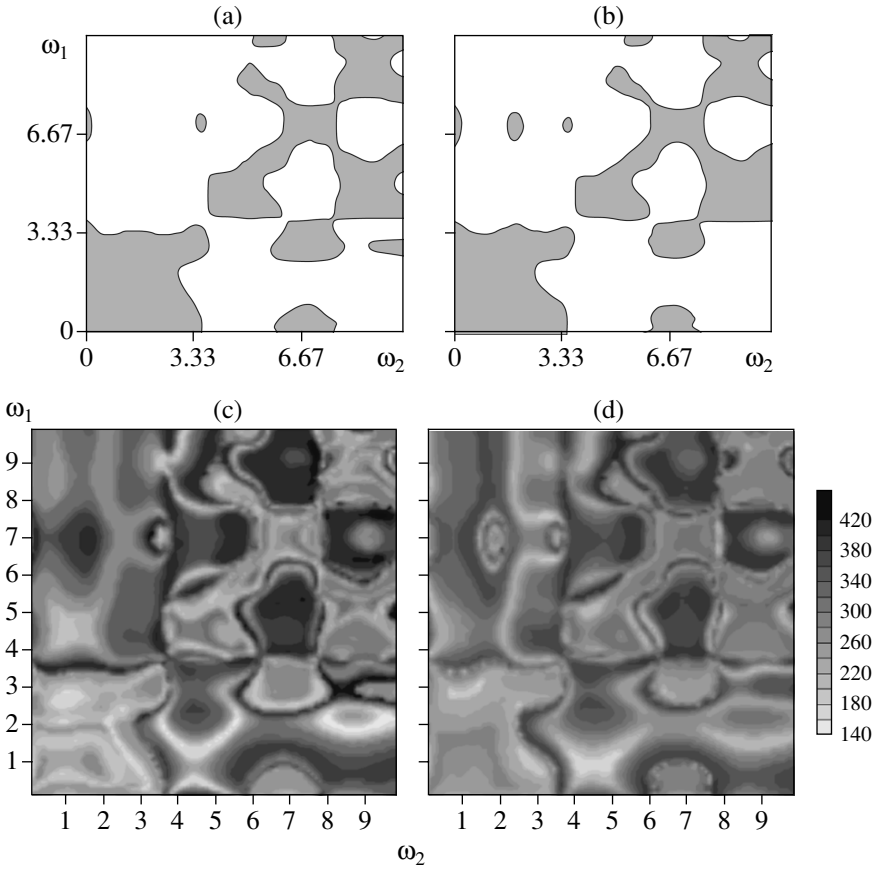

Fig. 4. (a, b) Basins of attraction for the slow (white area) and fast (gray area) states and duration of the transient process preceding these states of the CWGS gyro-BWT systems shown on the initial condition plane (f_1, f_2) (see formula (16)) for α = (c) 0.8 and (d) 1.0.

of the states is realized in the case of an arbitrary initial perturbation of the fields in coupled transmission lines. Therefore, it is of interest to analyze a certain class of initial field distributions in coupled transmission lines without limiting the consideration to the prevailing excitation of a slow (14) or fast (15) wave at the initial moment. In order to investigate the attraction basins for each of the stable (slow and fast) states of a CWGS gyro-BWT, we chose initial conditions of the form

$$\begin{aligned} F_1(\tau = 0, \xi) &= \delta^0 \sin(\omega_1 \pi(1-\xi)/2), \\ F_2(\tau = 0, \xi) &= \delta^0 \sin(\omega_2 \pi(1-\xi)/2). \end{aligned} \quad (16)$$

The realization of the bistable states was investigated at $A = 3.0$, $\mu_1 = 2.0$, $\mu_2 = 3.0$, and various coupling coefficients α.

Figures 4a–4d show the configurations of the attraction basins of the slow and fast states of the system on the (ω_1, ω_2) plane and the duration of the transient process T_t at two values of the coupling coefficient. The duration of the transient process is indicated in the figures by gradations of gray. Expressed in conventional units (100 conventional units correspond to approximately 10 RF oscillation periods), this duration is shown on the scale beside the plots. It follows from Fig. 4 that, with sufficiently arbitrary initial distributions of RF fields $F_{1,2}(\tau = 0, \xi)$ the boundaries of the attraction regions for each of the states of the coupled system have complicated shapes. Therefore, realization of one or the other oscillation mode in a coupled system is a challenge if no special measures are taken to excite the desired slow or fast normal wave.

It also follows from Fig. 4 that the duration of the transient process preceding stationary oscillation in a coupled system strongly depends on the choice of the initial conditions. Let us note at once that the duration of the transient process sharply increases at the boundaries of the attraction regions for the slow and fast states of a CWGS gyro-BWT. However, inside the attraction region for each of the stable states, the dependence of the duration of the transient process on the initial conditions is also complicated. Earlier [34, 35], a similar complicated dependence of transient processes on initial conditions was discovered for discrete-time systems with a small number of degrees of freedom (mappings). On a map showing the transient process durations as a function of initial conditions (Fig. 4), we can

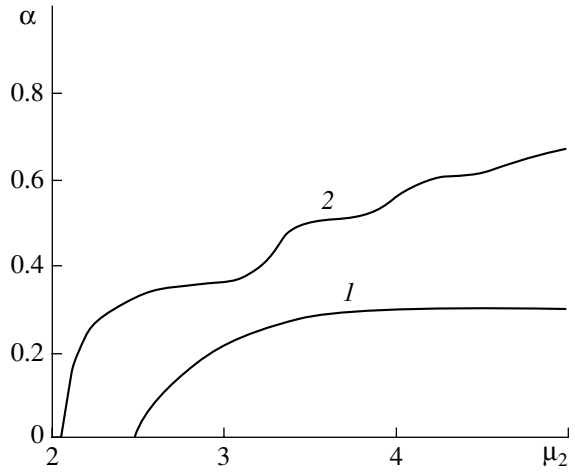

Fig. 5. Region of synchronization of joint oscillations of CWGS gyro-BWTs on the nonisochronism parameter μ_2—coupling coefficient α plane obtained at $\mu_1 = 2.0$; $A = (1)$ 3 and (2) 4.

clearly identify the initial conditions corresponding to the minimum duration of the transient process preceding stationary oscillation (white areas, in which the duration of transient processes is less than ten RF oscillation periods). Note that transient process duration $\langle T_t \rangle$ averaged over the ensemble of the initial conditions of form (16) slowly increases with coupling coefficient α. Simultaneously, the difference between the maximum and minimum durations of the transient processes decreases. For example, when the coupling coefficient doubles (from $\alpha = 0.5$ to $\alpha = 1.0$), the mean duration of the transient process increases, approximately, by 10%.

3. SYNCHRONIZATION OF SELF-OSCILLATIONS IN CWGS GYRO-BWTs

Let us investigate the synchronous modes of CWGS gyro-BWTs. In Fig. 5, quasi-synchronization zones are shown on control-parameter plane (μ_2, α) for various values of dimensionless tube length A. In [9, 10, 36], the nonautonomous dynamic modes in a self-oscillatory system that are characterized by external-signal locking of the oscillation base frequency are referred to as quasi-synchronization modes. In this case, the behavior of the oscillation amplitude may be rather complicated and exhibit features typical of both periodic and chaotic automodulation.

The regions of joint oscillation synchronization in CWGS gyro-BWTs are located higher than the corresponding line on the parameter plane. In the quasi-synchronization region, the base frequencies generated by each of the gyro-BWTs after cessation of the transient process become equal: $\omega_1 = \omega_2$. In this case, output field amplitudes $|F_{1,2}|$ of either gyro-BWT may exhibit various complex oscillations.

The regions of synchronous oscillations coincide for both the fast and slow states of the system; therefore, Fig. 5 corresponds to the case in which the initial conditions are specified by either (14) or (15). The synchronous oscillation frequencies for the fast and slow states of the system differ (see Fig. 3, curves *2* and *3*). A comparison of Figs. 3a and 3c with Figs. 3b and 3d shows that the synchronous oscillation frequencies differ in different multistable states and, as the coupling coefficient increases, approach the mean frequency $f \approx (f(\mu_1) + f(\mu_2))/2$ of autonomous oscillation at anisochronism parameters μ_1 and μ_2. Let us also note that, in the quasi-synchronization region, jumps in the frequency of the output signal are typical of the slow state of the coupled system when the control parameters of each of the partial systems and the coupling between these systems are varied (see Figs. 3b and 3d).[1] These jumps are caused by the competition between the fast and slow normal waves in the system, which makes the coupled system hop from the fast to the slow state and vice versa. These jumps are observed only when the excitation of the slow normal wave prevails, i.e., when the initial conditions are specified as (14). When the length of the system is large, several jumps occur as the coupling coefficient increases (see Fig. 3d). Therefore, in order to ensure stable frequency tuning in a coupled system by means of varying the coupling coefficient of the waveguiding systems, the fast state should be provided by the appropriate parameters of the device.

Again, let us turn to Fig. 5, which shows the boundary of the CWGS gyro-BWT quasi-synchronization region. It follows from the figure that mutual synchronization of two gyro-BWTs occurs when the coupling between the waveguiding systems is weak and the difference between the autonomous oscillation frequencies of each of the partial systems is small (the difference between the nonisochronism parameters $\Delta\mu = |\mu_1 - \mu_2|$ is small). As $\Delta\mu$ increases, the quasi-synchronization mode is realized at higher values of coupling coefficient α; i.e., the synchronous-oscillation region on plane (μ_2, α) narrows. The greater this narrowing, the greater dimensionless length of the gyrotube A (compare the boundaries of the quasi-synchronization region in Fig. 5 plotted at $A = 3.0$ and 4.0). As parameter A increases, the shape of the synchronization region boundary becomes irregular, due to competition between the modes with different spatial distributions of fields $|F_{s,f}|$ of the coupled system normal waves at the boundary of the synchronization region.

The complicated shape of the quasi-synchronization region of joint oscillations in CWGS gyro-BWTs is closely related to the output signal-automodulation modes. Therefore, in the next section, we briefly consider the automodulation modes that are realized in the coupled system under variations of the control parameters. It should be noted that the pattern of changes in the

[1] The frequency jumps are accompanied by amplitude jumps of the output signals of either coupled gyro-BWT.

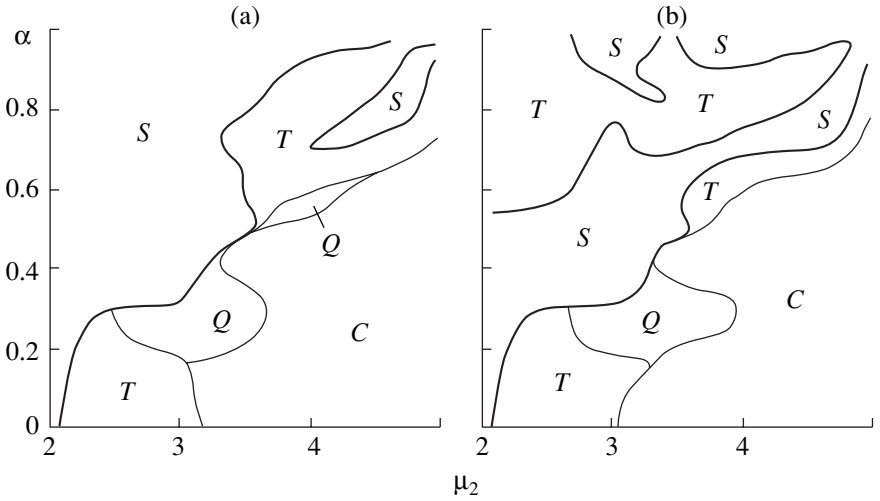

Fig. 6. Regions of stationary oscillation and output signal automodulation for the CWGS gyro-BWT joint oscillations on the nonisochronism parameter μ_2—coupling coefficient α plane obtained at $\mu_1 = 2.0$ for the (a) fast and (b) slow states at $A = 4.0$: (area *S*) stationary oscillation, (*T*) periodic automodulation of the output signal, (*Q*) complex periodic automodulation, and (*C*) chaotic oscillations.

CWGS gyro-BWTs oscillation modes depends on which multistable state the system is in.

4. NONLINEAR DYNAMICS IN A SYSTEM OF COUPLED CWGS GYRO-BWTs

Figure 6 shows the mode maps on the (μ_2, α) parameter plane plotted for the fast and slow states of a system with a dimensionless length of the interaction space $A = 4.0$. It can be seen in the figure that the boundaries of the regions of stationary oscillation and automodulation have complicated and highly irregular shapes. As in the case of gyro-CWGS BWTs such that the electron beam passes through only one of the coupled wave-guiding structures [37, 38] and in the case of a carcinotron [39, 40], these boundaries are formed by the stable multihump distributions of the field amplitude realized in each of the tubes at a long length of the system. The multihump distributions result from the competition between the phase and inertial nonlinearity mechanisms in the spiral beam interacting with the backward wave. The stability of the multihump spatial distributions is determined by the value of the coupling coefficient and the frequency difference between the coupled gyro-BWTs. Therefore, the complicated shape of the boundary of the stationary oscillation region, as well as that of the quasi-synchronization region, is determined by the stability of occurring states $F_{1,2}(\xi, \tau)$ and $I_{1,2}(\xi, \tau)$. These states result from repeated phase rebunching of the electron oscillators in the spiral electron beam over the length of the tube.[2]

[2] Note that, at $A = 3.0$, no shapes as complicated as those of the quasi-synchronization region (see Fig. 5) or of the stationary oscillation region are observed. This is because the shape of the field distribution in the tube is simpler when the system is not long.

The following point is of importance when a gyro-BWT is used as a high-power frequency-tunable millimeter-wave oscillator: the region of stationary oscillation in the case of a coupled system is wider than in the case of autonomous oscillation. For instance, at $A = 4.0$, the output signal automodulation in an autonomous gyro-BWT occurs at $\mu_{out} \approx 2.8$. In a CWGS gyro-BWT (Fig. 6), the stationary oscillation occurs at considerably higher values of parameter μ. In the fast state, the stationary oscillation is observed at the coupling coefficients $\alpha > 0.3$ and $\mu_2 < 3.5$. There is also a comparatively narrow region of stationary oscillation at $\alpha \in (0.7,1.0)$ and $\mu_2 > 4.0$. When the coupled system is in the slow state, the region of stationary oscillation occupies a smaller area on the control parameter plane and its boundary is much more complicated. In the stationary oscillation modes, quasi-synchronization of oscillations is observed in each of the gyro-BWTs, which allows an effective increase in the system total output power in the single-frequency mode of oscillation.

During transition to the automodulation mode, various types of fluctuation of output field amplitude $|F_{1,2}|$ are observed in the coupled system. Thus, near the boundary of the stationary oscillation region, automodulation is regular and periodic (areas *T* and *Q* in Fig. 6). When detuning $\Delta\alpha$ is large and coupling coefficient α is less than 0.6, the system exhibits chaotic oscillations (area *C* in Fig. 6). By varying coupling parameter α, we can effectively vary the spectral composition of a noise signal (i.e., its bandwidth, frequency, and spectral irregularity), which enables one to regard a system of coupled gyro-BWTs as a promising source of controllable millimeter-wave noise signal.

It should be noted that, in CWGS gyro-BWTs, the total efficiency of conversion of the energy of spiral

beam electron oscillators into the RF field energy (electron efficiency η_Σ), which is defined as

$$\eta_\Sigma = 1 - \frac{1}{4\pi}\int_0^{2\pi}(|\beta_1|^2 + |\beta_2|^2)d\theta_0, \quad (17)$$

substantially depends on coupling coefficient α. For nonstationary oscillation modes, formula (17) defines the oscillation efficiency incorrectly, a time-averaged value,

$$\langle\eta_\Sigma\rangle = \frac{1}{T}\int_{t_0}^{t_0+T}\eta_\Sigma(\tau)d\tau, \quad (18)$$

which determines the efficiency of the energy exchange in the system averaged over time interval T, must be used.

The analysis has shown that the maximum efficiency is realized at the coupling coefficients $\alpha > 0.5$–0.7, which is due to the optimum RF field structure formed in the interaction spaces of each of the partial systems. The optimum field distribution corresponds to the case in which the RF field amplitude increases in the direction of the tube collector end as compared to the case of the uncoupled system. As a result, electron oscillators phase-bunched at the end of the interaction space lose energy to the RF field more efficiently. The increase in the efficiency and in optimum coupling between the waveguiding structures strongly depends on the parameters of each of the gyro-BWTs. In the optimum case, the electron efficiency is $\eta_{max} \approx 1.5\eta_{\Sigma 0}$, where $\eta_{\Sigma 0}$ is the total oscillation efficiency of the uncoupled (autonomous) gyro-BWT, within the aforementioned range of parameters. Below, we summarize the values of total electron efficiency η_{max} and coupling parameter α_{opt}, at which they are achieved, depending on nonisochronism parameter μ_2, with the other parameters of the system being $A = 3.0$ and $\mu_1 = 2.0$. In addition, we present the values of the generation efficiency in the autonomous system ($\eta_{\Sigma 0}$).

μ_2	α_{opt}	η_{max}	$\eta_{\Sigma 0}$
3.0	0.92	0.23	0.17
4.0	0.94	0.26	0.18
5.0	0.66	0.22	0.19

CONCLUSION

In this work, the physical phenomena that are observed when spiral electron beams interact with RF fields of coupled waveguiding structures have been analyzed in the case of a cyclotron resonance with counter-propagating waves. The obtained results suggest the possibility of developing oscillators based on backward-wave cyclotron-resonance masers (CRMs) with coupled transmission lines. That synchronous single-frequency oscillation modes can be realized in a system of coupled gyro-BWTs is of great importance. Simultaneously, an increase in the electron efficiency of the coupled system, as compared to the total generation efficiency of autonomous gyro-BWTs, is observed at the same parameter values. It proves possible to make the device lighter and smaller than a tube with the same output power and a single higher-power beam. This can be achieved by reducing the sizes of the power supplies and magnetic system, which contribute to the weight and overall dimensions of the device most substantially.

The present work is not a comprehensive study of all the phenomena observed in CWGS gyro-BWTs. The possibility of selective excitation of the fast and slow normal waves in the system and the effect of a spatial charge on the processes in the system (the latter may be considerable for the four-wave interaction considered in this paper) call for further analysis. Finally, it is of interest to investigate CWGS gyro-BWTs with a variable waveguiding system geometry and shaped magnetic field, which would allow a higher generation efficiency and a wider frequency band of the oscillator under consideration [2, 3, 41].

It seems reasonable to consider electron devices with coupled transmission lines a promising separate class of active microwave devices [21]. Investigation of these coupled systems, as applied to devices that generate and amplify RF energy under cyclotron resonance conditions, will permit further optimization and improvement of the parameters of gyrodevices. For example, application of coupled waveguiding structures may provide for a more efficient method of enhancing the efficiency of gyro-BWTs relative to that of gyro-BWTs using irregular waveguides and a magnetic field varying along the gyrotube length.

ACKNOWLEDGMENTS

This work was supported by the Russian Foundation for Basic Research (project no. 02-02-16351), the program "Universities of Russia—Fundamental Research" (project no. UR.01.01.051), the Dynastiya Foundation for Nonprofit Programs, and the International Center of Fundamental Physics in Moscow.

REFERENCES

1. K. L. Felch, B. G. Danly, H. R. Jory, *et al.*, Proc. IEEE **87**, 752 (1999).
2. A. T. Lin, Phys. Rev. A. **46**, 4516 (1992).
3. C. S. Kou, C. H. Chen, and T. J. Wu, Phys. Rev. E. **57**, 7162 (1998).
4. S. H. Chen, K. R. Chu, and T. H. Chang, Phys. Rev. Lett. **85**, 2633 (2000).
5. J. Rodgers, H. Guo, G. S. Nusinovich, and V. L. Granatstein, IEEE Trans. Plasma Sci. **48**, 2434 (2001).

6. G. S. Nusinovich, W. Chen, and V. L. Granatstein, Phys. Plasmas **8**, 631 (2001).
7. G. S. Nusinovich, O. V. Sinitsyn, and A. Kesar, Phys. Plasmas **8**, 3427 (2001).
8. G. S. Nusinovich, A. N. Vlasov, and T. M. Antonsen, Phys. Rev. Lett. **87**, 218301-1 (2001).
9. D. I. Trubetskov and A. E. Khramov, Pis'ma Zh. Tekh. Fiz. **28** (18), 34 (2002) [Tech. Phyz. Lett. **28**, 767 (2002)].
10. D. I. Trubetskov and A. E. Khramov, Izv. Ross. Akad. Nauk, Ser. Fiz. **66**, 1761 (2002).
11. A. V. Gaponov, Izv. Vyssh. Uchebn. Zaved. Radiofiz. **2**, 443 (1959).
12. A. V. Gaponov, Izv. Vyssh. Uchebn. Zaved. Radiofiz. **2**, 450 (1959).
13. A. V. Gaponov, Izv. Vyssh. Uchebn. Zaved. Radiofiz. **4**, 547 (1961).
14. V. K. Yulpatov, Vopr. Radio Elektron., Ser. 1: Elektron., No. 12, 15 (1965).
15. V. K. Yulpatov, Vopr. Radio Elektron., Ser. 1: Elektron., No. 12, 24 (1965).
16. *Gyrotron* (Collection of Scientific Papers) (IPF Akad. Nauk SSSR, Gorky, 1981) [in Russian].
17. Z. G. Chen and H. Döring, Int. J. Infrared Millimeter Waves **5**, 691 (1984).
18. A. Yu. Dmitriev, D. I. Trubetskov, and A. P. Chetverikov, Izv. Vyssh. Uchebn. Zaved. Radiofiz. **34**, 595 (1991).
19. D. I. Trubetskov and A. P. Chetverikov, Izv. Vyssh. Uchebn. Zaved., Prikl. Nelin. Din. **2** (5), 3 (1994).
20. V. A. Isaev, V. L. Fisher, and A. P. Chetverikov, in *Lectures on Microwave Electron.and Radio Phys. 7th Winter Workshop for Engineers* (Saratov Gos. Univ., Saratov, 1986), Book 2, p. 3.
21. D. I. Trubetskov, in *Lectures on Microwave Electron. and Radio Phys. 4th Winter Workshop for Engineers* (Saratov Gos. Univ., Saratov, 1978), Book 5, p.89.
22. V. A. Balakirev, A. O. Ostrovskii, and Yu. V. Tkach, Zh. Tekh. Fiz. **61** (9), 94 (1991).
23. W. H. Louisell, *Coupled Mode and Parametric Electronics* (Wiley, New York, 1960).
24. D. I. Trubetskov and V. P. Shakhin, in *Microwave Electronics*, Ed. by V. N. Shevchik (Saratov Gos. Univ., Saratov, 1973), No. 7, p. 44.
25. S. P. Kuznetsov and D. I. Trubetskov, in *Backward-Wave-Tube Electronics*, Ed. by V. N. Shevchik and D. I. Trubetskov (Saratov Gos. Univ., Saratov, 1975), p. 135 [in Russian].
26. R. W. Hockney and J. W. Eastwood, *Computer Simulation Using Particles* (McGraw-Hill, New York, 1981).
27. P. J. Roache, *Computational Fluid Dynamics* (Albuquerque, N.M., Hermosa, 1972).
28. M. I. Rabinovich and D. I. Trubetskov, *Introduction to Theory of Oscillations and Waves*, 3rd ed. (RKhD, Moscow, 2000) [in Russian].
29. V. V. Astakhov, B. P. Bezruchko, E. N. Erastova, and E. P. Seleznev, Zh. Tekh. Fiz. **60** (10), 19 (1990).
30. A. S. Dmitriev, S. O. Starkov, and M. E. Shirokov, Izv. Vyssh. Uchebn. Zaved., Prikl. Nelin. Din. **4** (4/5), 40 (1990).
31. Y. Liu and P. Davis, Int. J. Bifurcation and Chaos **8**, 1686 (1998).
32. N. S. Ginzburg and M. I. Petelin, Izv. Vyssh. Uchebn. Zaved., Prikl. Nelin. Din. **2** (6), 3 (1994).
33. V. L. Bratman and A. V. Savilov, Izv. Vyssh. Uchebn. Zaved., Prikl. Nelin. Din. **2** (6), 27 (1994).
34. A. A. Koronovskii, D. I. Trubetskov, A. E. Khramov, and A. E. Khramova, Dokl. Akad. Nauk **383**, 322 (2002) [Dokl. Phys. **383**, 181 (2002)].
35. A. A. Koronovskii and A. E. Khramov, Pis'ma Zh. Tech. Fiz. **28** (15), 61 (2002) [Tech. Phys. Lett. **28**, 648 (2002)].
36. D. I. Trubetskov and A. E. Khramov, Radiotekh. Electron. (Moscow) **48**, 116 (2003) [J. Commun. Technol. Electron. **48**, 105 (2003)].
37. A. A. Koronovskii and A. E. Khramov, Pis'ma Zh. Tekh. Fiz. **29** (6), 63 (2003) [Tech. Phys. Lett. **29**, 510 (2003)].
38. A. A. Koronovskii, D. I. Trubetskov, and A. E. Khramov, Zh. Tekh. Fiz. **73** (6), 110 (2003) [J. Tech. Phys. **48**, 768 (2003)].
39. D. I. Trubetskov, V. G. Anfinogentov, N. M. Ryskin, *et al.*, Radiotekhnika (Moscow) **63** (4), 61 (1999).
40. N. M. Ryskin and V. N. Titov, Izv. Vyssh. Uchebn. Zaved., Radiofiz. **42**, 566 (1999).
41. V. L. Bratman, S. L. Novozhilov, and M. I. Petelin, Elektron. Tekh., Ser. 1: Elektron. SVCh, No. 11, 46 (1976).